LAWRENCE
LIVERMORE
NATIONAL
LABORATORY

LLNL-JRNL-648594

Magnetic collimation of relativistic positrons and electrons from high intensity laser - matter interactions

H. Chen, G. Fiksel, D. Barnak, P. Y. Yu, R. F. Heeter, A. Link, D. D. Meyerhofer

January 21, 2014

Physics of Plasmas

Disclaimer

Magnetic collimation of relativistic positrons and electrons from high intensity laser–matter interactions

Hui Chen1, G. Fiksel2, D. Barnak2, P. Y. Chang2, R. F. Heeter1, A. Link1 and D. D. Meyerhofer2

1. Lawrence Livermore National Laboratory, Livermore, CA 94551

2. Laboratory for Laser Energetics, University of Rochester, Rochester, NY 14623

Abstract:

Collimation of positrons produced by laser-solid interactions has been observed using an externally applied axial magnetic field. The collimation leads to a narrow divergence positron beam, with an equivalent FWHM (full width at half maximum) beam divergence angle of 4° *vs* the un-collimated divergence of about 20°. A fraction of the laser-produced relativistic electrons with energies close to those of the positrons is collimated, so the charge imbalance ratio (n_{e-}/n_{e+}) in the co-propagating collimated electron-positron jet is reduced from ~100 (no collimation) to ~2.5 (with collimation). The positron density in the collimated beam increased from 5×10^{7} cm^{-3} to 1.9×10^{9} cm^{-3}. This is a significant step towards the grand challenge of making a charge neutral electron-positron pair plasma jet in the laboratory.

PACS number(s): 52.38.Ph.; 52.55.-s; 52.27.Ep; 52.27.Ny

Relativistic electron-positron pair plasmas and jets exist in many astrophysical objects and are invoked to explain energetic phenomena related to Gamma Ray Bursts, Active Galactic Nuclei, and Black Holes [1-7]. Pair plasmas are important in fundamental plasma physics because of unique properties [8-10] resulting from mass symmetry. On Earth, positrons and positron plasmas from radioactive isotopes or accelerators are studied extensively at low energies (sub-MeV) in areas related to surface science, positron emission tomography, basic antimatter science such as antihydrogen experiments [8], and Bose-Einstein condensed positronium [11]. The creation of dense, relativistic pair plasmas has been elusive, due to the difficulty of producing pairs in high density and the short positron lifetime [12]. To date, there is no technique to produce the high temperature pair plasmas and high-flux pair jets required to simulate astrophysical phenomena, or study many fundamental pair plasma properties.

In recent years, high-energy ultra-short lasers have made jets of mega-electron-volt (MeV) positrons and electrons in a small volume (< 3 mm^3) [13], with particle densities about 10^{15} cm^{-3} and 10^{13} cm^{-3} at the source for electrons and positrons [14], respectively. To make a true pair plasma, three conditions must be satisfied: (i) the MeV particles must be confined longer than the plasma timescale of interest (e.g. oscillations); (ii) the plasma dimensions must be significantly greater than the Debye length; and (iii) the plasma must be charge neutral. Condition (ii) has previously been achieved experimentally [14], but (i) and (iii) have not been demonstrated, since the pair jets were previously not confined and the laser-driven electron density typically exceeds the positron density by about 2 orders of magnitude.

Magnetic confinement of a laser-produced pair plasma, (for example proposed by Myatt *et al*. [12]), offers a promising path to achieving conditions (i) and (iii). The first step is to collimate the pair jets, transporting the particles of interest away from the complex laser-target source while increasing the particle density. With the particles collimated, further steps can then be taken.

While the effect of magnetic B-fields on laser-driven plasmas has been extensively studied in the past decade, for applications including inertial confinement fusion [15-17], electron fast-ignition [18-20], and proton beam generation [21, 22], little attention has been given to relativistic electron-positron jets. Laser-plasma interactions have created 100 – 1000 T B-fields [23, 24]. It is difficult to apply such fields to short bursts of MeV positrons, due to the highly dynamic geometry of laser-driven B-fields [18-24]; it is difficult to coordinate both pair and B-field processes on few-ps timescales.

In this Letter, we show that, for the first time, a relativistic pair jet has been effectively collimated using magnetic fields from an external, pulsed Helmholtz-type coil, using the magneto-inertial fusion electrical discharge system (MIFEDS) [25]. An advantage of the external MIFEDS coil is that the B-field and pair beam generation processes are separated and characterized independently. The B-field duration is much longer (μs) than the beam duration (ps), so the field is stationary during the pair beam propagation. This enables systematic data to be taken for various controlled experimental conditions.

These experiments at the OMEGA EP laser facility [26] used 10 ps pulses at 1054 nm. The targets were plain gold discs, 1 mm thick and 2 mm in diameter. The laser power contrast was about 10^8 - 10^9 and measured on-shot focal spot data shows 80% of the laser energy contained within a 20±5 micron radius. The laser energies were 830+/-30 J. The

x-ray emission and laser-plasma coupling efficiency were monitored for shot-to-shot variations using a transmission crystal spectrometer (for Au Kα) and step-wedge filter pack (for bremsstrahlung up to 1 MeV) [27]. The Au K-alpha and bremsstrahlung yields varied within 10% for laser energies from 800 – 850 J. Two orthogonal magnetic electron-positron-proton spectrometers (EPPS) [28], one normal and one parallel to the rear of the target surface, measured the absolute energy and angular distributions of electrons and positrons from the laser-target interactions. While the parallel EPPS provided reference information, the EPPS normal to the target was aligned to the center of the pair jet emitted from the target and provided a direct measure of the collimation.

The energy and angular distribution of the electrons and positrons from the laser-target interaction were characterized. Fig. 1 shows the broad electron spectrum with a quasi-Maxwellian distribution at 5-8 MeV temperatures, versus quasi-monoenergetic positrons with typical energies of 12-15 MeV. The angular distribution shows a spread (FWHM) of about 30° and 20° for electrons and positrons respectively. The total number of electrons ($1\text{-}3\times10^{12}$) is about ~100 times higher than the total number ($1\text{-}4\times10^{10}$) of positrons. Near the peak in the positron energy spectrum, the electron spectral density is comparable. If this part of the spectrum is selected, the numbers of positrons and electrons are comparable.

Magnetic fields are commonly used both for energy selection (e.g. magnetic spectrometers) and for charged particle beam focusing (e.g. magnetic lenses). For this experiment, a small circular coil with an inner diameter of 6.6 mm (Fig. 2 inset) generates the magnetic field. The coil consists 4 loops of Kapton-insulated wire to carry a peak

current of 20 kA generated by MIFEDS with a pulse duration of ~2 μs, gaining a peak magnetic field on the coil axis is about 8 T.

The axisymmetric field created by the coil acts as a lens whose focal length depends on particle energy and magnetic field [29]:

$$f = 4 / \int dz \left[qB(z) / \gamma m v_z \right]^2 \sim \rho_{ce}^2 / a \,, \qquad [1]$$

where $\rho_{ce} = \gamma m v_z / qB_0$ is the Larmor radius evaluated at the peak magnetic field B_0, a is the coil radius, and the integral is along the z-axis. The focal length depends on the square of the electrical charge, so the magnetic focusing is identical for positrons and electrons.

Figure 2 shows calculated trajectories of positrons with a peak energy of 13 MeV (typical for these experiments), a width (FWHM) of 3 MeV, and an angular divergence (FWHM) of 20°. The coil, with peak axial B-field of 8 T, was placed 18 mm from the target. As a result of magnetic focusing, an initially diverging beam becomes nearly parallel, from the rear of the coil to the detector 579 mm away from the source.

The experimental data in Fig. 3 illustrate the effect of magnetic collimation for both electron and positron beams. The coil was 12 mm from the source and the EPPS spectrometer was 579 mm from the source. The peak positron signal in the EPPS increased about 50-fold relative to reference shots without MIFEDS. Similarly, the electron signal at the same energy increased about 30-fold.

Assuming no loss of positrons in the collimation process, and that the signal increases solely due to the reduced beam expansion, an upper bound of the effective divergence can be estimated. It would be less if there were positron losses. From the detected

positron numbers (1.5×10^{12} with MIFEDS and 6.3×10^{10} without) the effective divergence angle of the collimated beam is about 4° (FWHM), calculated as 2atan(r/L), where r = 22.5 is the collimated beam radius and L = 579 mm is the distance between positron source and the detector. The collimated beam divergence angle (4° FWHM) is a factor of 5 smaller than that of the un-collimated beam. This agrees with particle tracing simulations: the ratio of polychromatic distributed particles observed in the detector with and without MIFEDS is about 40-50, and the divergence angle is reduced six-fold from 20° to 3°.

Since the detector is far from the target, the strongest focusing occurs for the part of the energy spectrum for which the focal distance (Eq. [1]) matches the source-to-coil distance. The data in Fig. 3 show that 13 MeV particles are best focused with the coil 12 mm from the target source, differing from the simulation results (Fig. 2) where to collimate 13 MeV particles the coil had to be positioned 18 mm from the target. The focusing strength of the coil appears to be higher than predicted from simulation. This does not change the main result of the paper of successful collimation of laser-produced positrons (and electrons). But the difference is substantial enough to warrant further investigation.

To better understand the effect of magnetic collimation, and to further optimize the focusing, this experiment was repeated using various source-to-coil distances. Varying this distance focuses different parts of the energy spectrum, and figures 4 and 5, show the dependence of both the peak energy and the signal level on the source-to-coil distance.

The peak energy dependence shows similar behavior for both electrons and positrons (Fig. 4), resulting from the magnetic focusing being independent of charge sign. The

slopes of the curves are slightly different; with the positron curve slope (~1 MeV/mm) steeper than the electron curve slope (~0.7 MeV/mm). This can be attributed to a radial electric field (E-field) originating in the non-neutral charged beam, where there are 2-3 orders of magnitude more electrons than positrons before the collimation. Near the source, n_e is $10^{14} - 10^{15}$ cm^{-3}; suggesting an E-field of up to 1 MeV/mm perpendicular to the beam axis, further focus positrons while defocusing electrons. Estimates indicate a radial E-field of just ~0.13 MeV/mm can explain the measured slope difference. A quantitative accounting for a laser-generated electric field is far more difficult than for an imposed magnetic field, as it must be determined self-consistently from the evolution of the electron and positron space charge.

The results of the analytical calculations and simulations for the peak energy of the focused particles, plotted in Fig. 4, show good agreement. The calculations and experimental results have a similar trend, although as previously mentioned the experimental focusing is stronger (offset vertically) relative to theory. Potential causes for this offset may include errors in the coil B-field strength, the EPPS energy calibration, the radial electric field effect, and misalignment of the magnetic coil and EPPS. Another possibility is modification of the coil vacuum magnetic field by the charged cloud expanding from the target.

Figure 5 shows the dependence of the measured electron and positron densities in the collimated jet on the source-to-coil distance. Both electron and positron densities increase weakly with the distance until ~15 mm, where they peak. Fig. 4 shows that at this distance the best focus is for particles near 15 MeV, at the peak of the positron energy distribution (Fig. 1 and Fig. 3.).

The electron-to-positron density ratio is greatly reduced with magnetic collimation. The species ratio in the collimated beam varies with coil position because the coil selectively collimates particles within a narrow energy range. With the coil position optimized for the positrons, only a fraction of electrons are selected from their exponential energy distribution (Fig. 3). Electrons outside of the energy range are deflected out of the collimated beam and do not reach the detector. Measured 0.6 m from the target, when collimation is used, beam densities of 1.9×10^{9} cm^{-3} and 4.7×10^{9} cm^{-3} are achieved for positrons and electrons, respectively, with both species' energy distribution centered around 13-14 MeV. In comparison, without collimation the beam densities are about 5×10^{7} cm^{-3} and 4×10^{8} cm^{-3} at 0.6 m from the source, respectively. With collimation, the charge ratio (n_e-/n_e+) in the electron-positron beam is about 2.5, and charge neutrality is improved by a factor of 40 compared to the previously reported charge ratio of ~100 [14].

Using the data from Fig. 3 and Fig. 5, the parameters in the collimated electron-positron beam for creating a pair plasma can be estimated. The temperatures for electrons (T_e) and positrons (T_p) can be estimated from the distributions. In the longitudinal direction, T_e ~2 MeV, and T_p ~1 MeV; while in the transverse direction, $T_e = T_p$ ~ 0.2 MeV. Using the density shown in Fig. 4, the Debye length ~ 3 cm for $T_{e/p}$= 0.2 MeV. This is comparable to the beam diameter (~4 cm at the detector) and approximately satisfies plasma condition (ii) described above; this becomes increasingly true if the temperature is reduced below 200 keV. There are 10^{7}-10^{9} particles inside the Debye sphere, satisfying that measure of a relativistic plasma.

In addition to being larger than the Debye length, and having many particles within a Debye sphere, a true pair plasma must also be confined for sufficient time for collective

behaviors to emerge, per condition (i) described above. For example, a few plasma oscillation periods (τ_e) should be sufficient to enable plasma effects to develop for basic plasma physics studies. For the above plasma conditions, τ_e~3 ns, equivalent to a transit length $\tau_e c$~100 cm. In the experiment, the coil-to-detector distance, ~58 cm, might already be sufficient for collective behavior to develop as the jet propagates. With magnetic collimation, the relativistic pair jet satisfies (approximately) the pair-plasma conditions (i) through (ii), and has demonstrated 40-fold improvement in the charge neutrality condition (iii).

With further improvements, these jets become usable in astrophysically relevant laboratory experiments. Simulations have demonstrated that collisionless shocks can be produced by two counter-propagating relativistic pair plasma jets [30]. Particles accelerated in the shocks have been proposed as the origin of most non-thermal high-energy emission seen from jets in astrophysical events [1-7]. To effectively create shocks within laboratory length scales (cm), simulations indicate the pair plasma density should be 10^{13} to 10^{17} cm^{-3} [30] depending on interaction length, and the jet energy 10-100 MeV. The present pair jets meet the energy requirement but appear insufficiently dense. The pair plasma density needs to be increased by orders of magnitude to observe collisionless-shock interactions for astrophysics.

To achieve the desired density, the number of pairs may be increased, and the plasma volume may be reduced. For the former, one could increase the driving laser energy and further optimize the laser-target interaction. For the latter, an improved magnetic field system is needed: options include either a stronger MIFEDS-like magnetic field, superconducting quadrupole magnets as used in accelerators, or laser driven magnetic

fields [22]. As a next step for pair plasma confinement, a magnetic mirror cell ~10 cm in size is another promising candidate. If the particles are confined for several bounce times, this would further increase the plasma density and decrease the Debye length, reducing boundary effects relative to bulk plasma properties. But for relativistic jets, a high magnetic field will be required for good plasma confinement.

Systematic studies are needed to realize any of these. With continued advances in high-power short-pulse laser technology [31] and further understanding of the physical properties of laser produced pair jets, a dense relativistic pair plasma could be achieved in the laboratory.

In summary, magnetic collimation of laser produced relativistic positron and electron jets has been achieved using an external magnetic field. The resulting beams are near parallel, with vastly improved charge neutrality, bringing the prospect of charge-neutral relativistic pair-plasma physics experiments tantalizingly close. The physics process is well understood. Based on these results and with further effort, a confined, charge-neutral, relativistic pair plasma may be achieved using the mirror fields provided by a double coil. Such progress will lead to future laboratory astrophysical experiments as well as basic plasma physics experiments.

Acknowledgement: We gratefully acknowledge the support of the Omega EP facility during these Laboratory Basic Science experiments. We thank Bob Cauble, Henry Shaw and Bill Goldstein for encouragement and support, and D.D. Ryutov for fruitful discussions. This work was performed under the auspices of the U.S. DOE by LLNL under Contract DE-AC52-07NA27344, and funded by the LDRD (12-ERD-062) program.

[1] E. Fermi, Phys. Rev. **75**, 1169 (1949)

[2] A. R. Bell, MNRAS **182**, 147 (1978)

[3] R. Blandford, and J. Ostriker, Astrophysics. J **221**, L29 (1978)

[4] P. Meszaros, Annal Review of Astronomy and Astrophysics **40**, 137 (2002).

[5] J. Wardle, et al., Nature **395**, 457 (1998)

[6] A. Spitkovsky, Astrophysics. J. Lett. **673**, L39 (2008)

[7] G. Weidenspointner, et al., Nature **451**, 159 (2008).

[8] V. Tsytovich and C. B. Wharton, Comments Plasma Phys. Controlled Fusion **4**, 91 (1978).

[9] A. Bret, L. Gremillet, and M. E. Dieckmann, Phys. Plasmas, 17, 120501 (2001).

[10] C. M. Surko and R. G. Greaves, Phys. Plasmas **11**, 2333 (2004).

[11] E. P. Liang and C. D. Dermer, Opt. Commun. **65**, 419, (1988); A. P. Mills, Jr., Nucl. Instrum. Methods Phys. Res., Sect. B **192**, 107 (2002).

[12] J. Myatt, J. A. Delettrez, A. V. Maximov, D. D. Meyerhofer, R. W. Short, C. Stoeckl, and M. Storm, Phys. Rev. E **79**, 066409 (2009).

[13] Hui Chen, S. Wilks, D. Meyerhofer, J. Bonlie, C. Chen, S. Chen, C. Courtois, L. Elberson, G. Gregori, W. Kruer, O. Landoas, J. Mithen, J. Myatt, C. Murphy, P. Nilson, D. Price, M. Schneider, R. Shepherd, C. Stoeckl, M. Tabak, R. Tommasini, and P. Beiersdorfer, Physical Review Letters **105**, 015003 (2010).

[14] Hui Chen, D. D Meyerhofer, S. C. Wilks, R. Cauble, F. Dollar, K. Falk, G. Gregori, A. Hazi, E. I. Moses, C. D. Murphy, J. Myatt, J. Park, J. Seely, R.

Shepherd, A. Spitkovsky, C. Stoeckl, C. I. Szabo, R. Tommasini, C. Zulick, P. Beiersdorfer, High Energy Density Physics **7**, 225 (2011)

[15] C. K. Li, F. H. Séguin, J. A. Frenje et al., Science **327**, 1231 (2010)

[16] M. Hohenberger, P. Y. Chang, G. Fiksel, J. P. Knauer, R. Betti, F. J. Marshall, D. D. Meyerhofer, F. H. Seguin, and R. D. Petrasso, Phys. Plasmas **19**, 056306, (2012).

[17] P. Y. Chang, G. Fiksel, M. Hohenberger, J. P. Knauer, R. Betti, F. J. Marshall, D. D. Meyerhofer, F. H. Seguin, and R. D. Petrasso, Phys. Rev. Lett. **107**, 035006, (2011).

[18] Y. Sentoku, E. d'Humieres, L. Romagnani, P. Audebert and J. Fuchs, Physical Review Letters **107**, 135005 (2011)

[19] R. H. H. Scott, et al., Physical Review Letters **109**, 015001 (2012)

[20] S. Chawla, et al., Physical Review Letters **110**, 025001 (2013)

[21] T. Toncian, et al., Science **312**, 410 (2006)

[22] S. Kar, et al., Physical Review Letters **106**, 225003 (2011)

[23] M. Tatarakis, et al., Nature **415**, 280 (2002)

[24] S. Fujioka, et al., Nature Scientific Reports **3**, 1170 (2013)

[25] O. G. Gotchev, et al., Rev. Sci. Instrum. **80**, 043504 (2009).

[26] L. J. Waxer, D. N. Maywar, J. H. Kelly, T. J. Kessler, B. E. Kruschwitz, S. J. Loucks, R. L. McCrory, D. D. Meyerhofer, S. F. B. Morse, C. Stoeckl, and J. D. Zuegel, Optical Photonics News **16**, 30 (2005).

[27] Hui Chen, R. Tommasini, J. Seely, C. I. Szabo, U. Feldman, N. Pereira, G. Gregori, K. Falk, J. Mithen, C. D. Murphy, Rev. Sci. Instrum. **83** 10E113 (2012)

[28] Hui Chen, N. L. Back, T. Bartal, F.N. Beg, D.C. Eder, A.J. Link, A.G. MacPhee, Y. Ping, P.M. Song, A. Throop, and L. Van Woerkom, Review of Scientific Instruments **79**, 033301 (2008).

[29] R. Egerton, *Physical Principles of Electron Microscopy*, p. 41, Springer, 2005.

[30] L. Sironi and A. Spitkovsky, Astrophysical J., 698, 1523 (2009); L. Sironi and A. Spitkovsky, Astrophysical J. **726**, 75 (2011).

[31] M. Dunne, HiPER – Technical Background and Conceptual Design Report (2007).

FIGURE CAPTIONS

Fig. 1: Measurements of electron and positron energy (a) and angular (b) distributions for 800 J, 10 ps laser beam interacting with 1 mm thick, 2 mm diameter gold targets.

Fig. 2: Ray-tracing simulation of magnetic collimation of 13 MeV positrons with an energy width of 3 MeV (FWHM) and divergence angle of 20° (FWHM). An approximately parallel beam is formed after the coil.

Fig. 3: Energy distributions of electrons and positrons with and without magnetic collimation. With collimation, peaked distributions were observed for both electron and positrons.

Fig. 4: Peak energies in the distribution of electrons and positrons as a function of the source-to-coil distance.

Fig. 5: The densities of electrons and positrons in the collimated beam measured at the detector location (579 mm from the source).

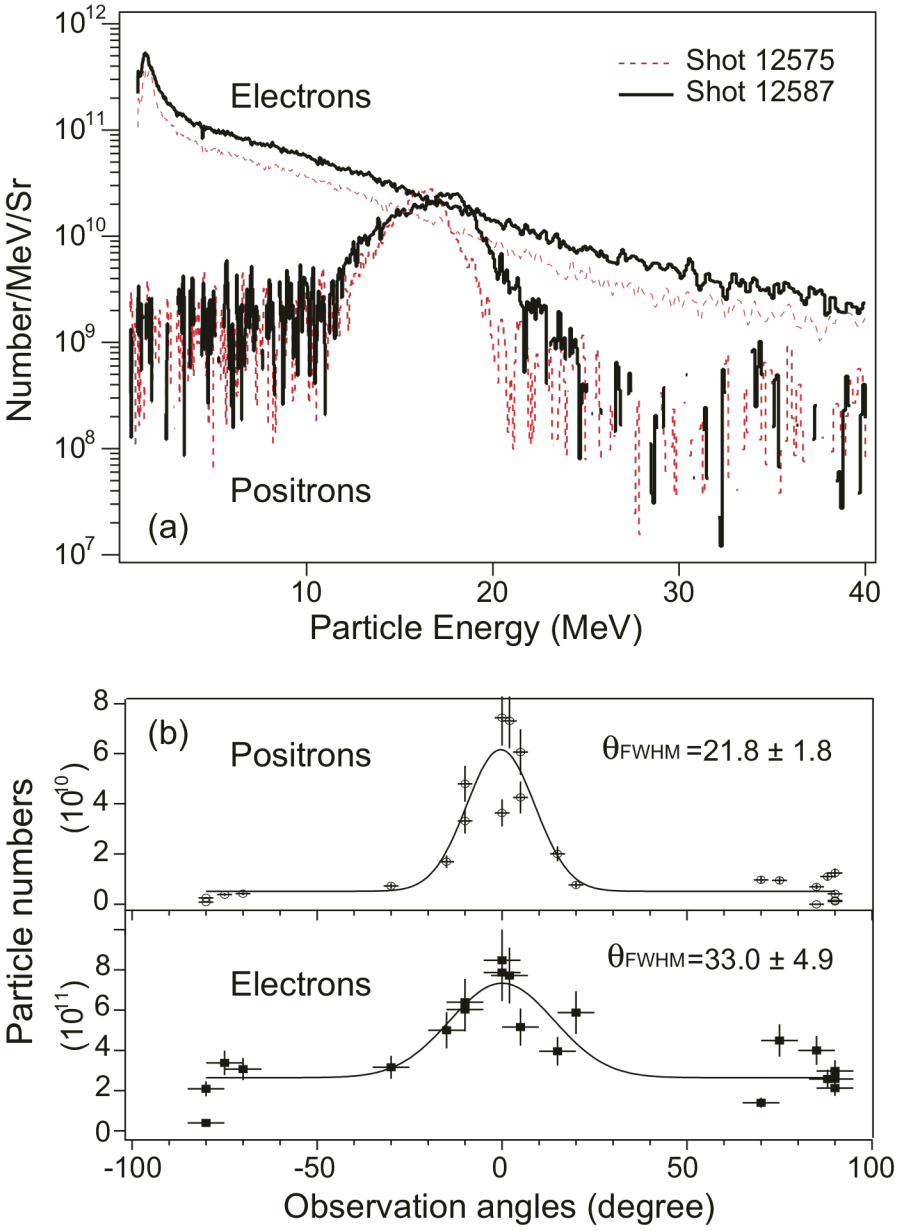

Fig. 1: Measurements of electron and positron energy (a) and angular (b) distributions for 800 J, 10 ps laser beam interacting with 1 mm thick, 2 mm diameter gold targets.

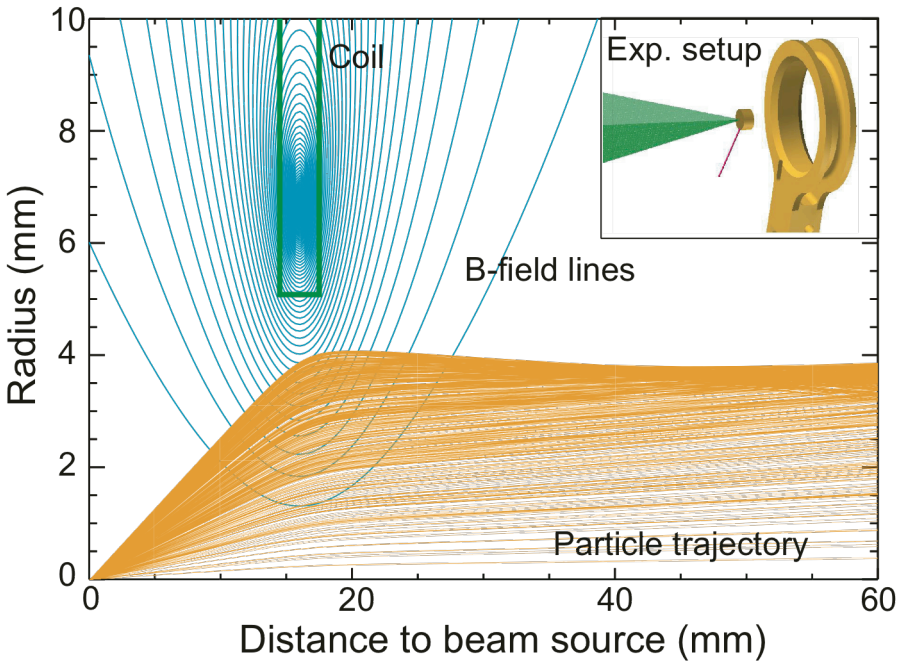

Fig. 2: Ray-tracing simulation of magnetic collimation of 13 MeV positrons with an energy width of 3 MeV (FWHM) and a divergence angle of 20° (FWHM). An approximately parallel beam is formed after the coil.

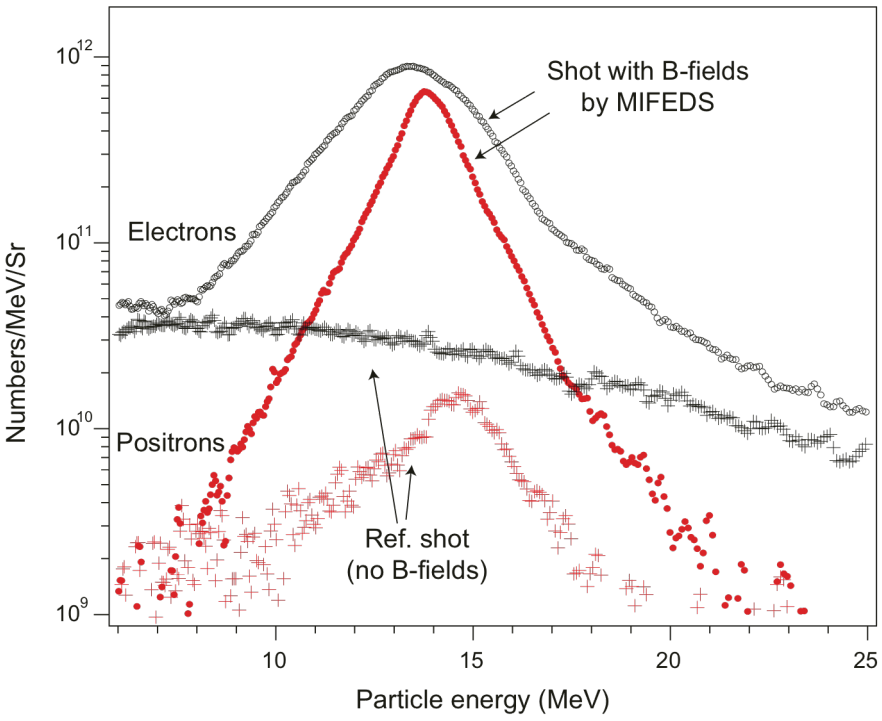

Fig. 3: Energy distributions of electrons and positrons with and without magnetic collimation. With collimation, peaked distributions were observed for both electron and positrons.

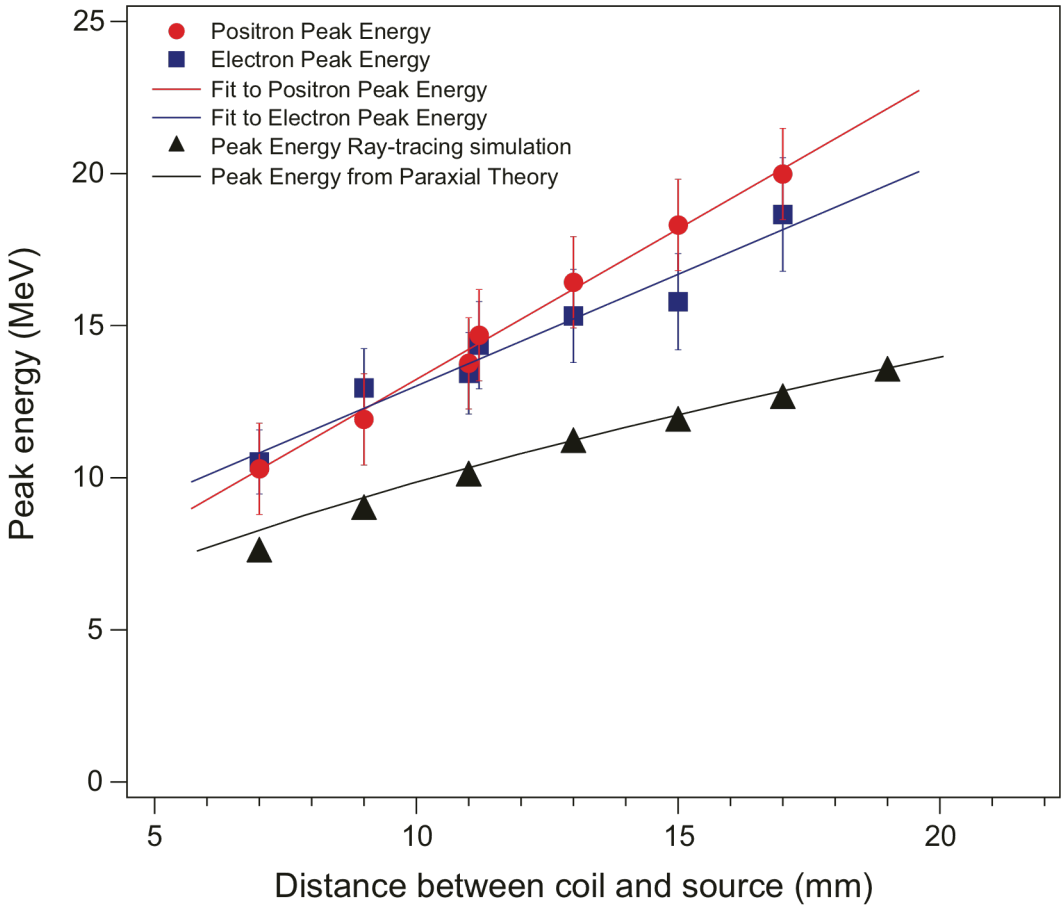

Fig. 4: Peak energies in the distribution of electrons and positrons as a function of the source-to-coil distance.

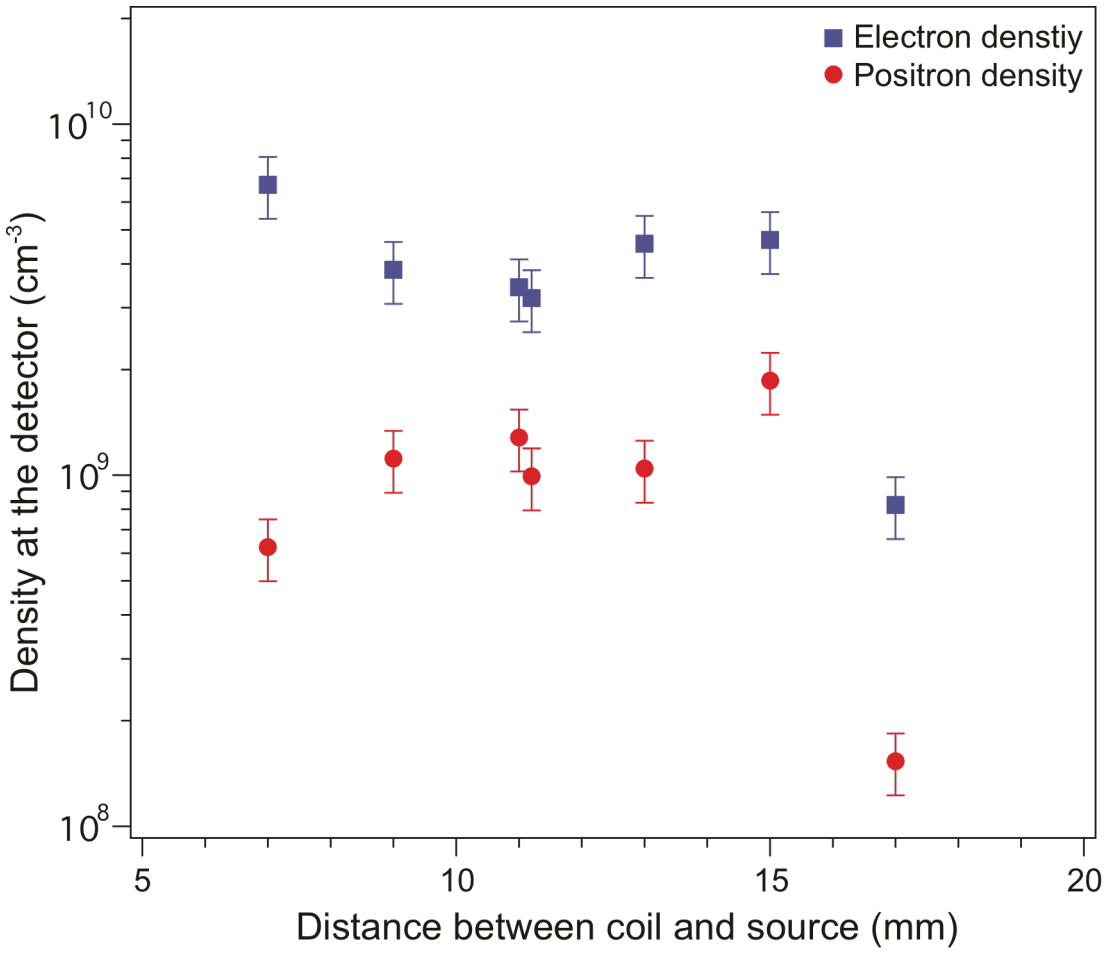

Fig. 5: The densities of electrons and positrons in the collimated beam measured at the detector location (579 mm from the source).